Magnetization dynamics in microscopic spin-valve elements: Shortcomings of the macrospin picture

F. Wegelin, D. Valdaitsev, A. Krasyuk, S. A. Nepijko, G. Schönhense, and H. J. Elmers*
Universität Mainz, Institut für Physik, D-55128 Mainz, Germany

I. Krug and C. M. Schneider
Institut für Festkörperforschung IFF-9, Forschungszentrum Jülich GmbH, D-52425 Jülich, Germany
(Received 12 September 2007; published 11 October 2007)

We have studied ultrafast magnetodynamics in micropatterned spin-valve structures using time-resolved x-ray photoemission electron microscopy combined with x-ray magnetic circular dichroism. Exciting the system with ultrafast field pulses of 250 ps width, we find the dynamic response of the free layer to fall into two distinctly different contributions. On the one hand, it exhibits localized spin wave modes that strongly depend on the shape of the micropattern. A field pulse applied perpendicular to the exchange bias field along the diagonal of a square pattern leads to the excitation of a standing spin wave mode with two nodes along the field direction. This mode is strongly suppressed for a pattern of elliptical shape. On the other hand, the integrated response of the free layer roughly follows a single-spin model with a damping constant of $\alpha = 0.025$ independent of the shape and resembles the response of a critically damped forced oscillator.

DOI: 10.1103/PhysRevB.76.134410 PACS number(s): 75.40.Gb, 75.60.−d, 75.75.+a

A magnetic spin valve (SV) represents a very important functional structure in modern magnetism. SVs are extensively used as read heads in magnetic storage devices. Their functionality depends crucially on the interplay of magnetic coupling phenomena. In its simplest version, a SV is composed of two ferromagnetic (FM) layers separated by a nonmagnetic (NM) spacer layer mediating a usually antiferromagnetic *indirect exchange coupling*,[1,2] which determines the magnetic configuration of the layer stack. In a more refined approach, the magnetization in one of the FM layers (hard layer) is additionally stabilized by a strong coupling (*exchange biasing*) to an antiferromagnet. The orientation of the magnetization vector in the other—the free—FM layer is then sensed by the giant magnetoresistance (GMR) effect.[2,3] In more complex systems, further coupling mechanisms such as orange peel or edge coupling may take place.[4] Thus, micron-sized spin valves are extremely interesting structures from a fundamental point of view, as they provide a unique access to the interplay between different types of magnetic coupling in both static and dynamic experiments.

Advanced magnetic recording schemes and spintronics push the switching time into the gyromagnetic regime. Ultrafast magnetization excitations in soft magnetic microstructures thus recently attracted particular attention.[5–10] New switching concepts involving the spin transfer torque[11,12] also rely on gyromagnetic processes. For microscopic elements with a small magnetic anisotropy and a well-defined shape, the high-frequency behavior is governed by confined spin wave eigenmodes.[5,6,13] Quantitatively, the magnetodynamic response may be described by the Landau-Lifshitz-Gilbert equation, $d\vec{M}/dt = -\gamma(\vec{M} \times \vec{H}_{eff}) + (\alpha/M_s)(\vec{M} \times d\vec{M}/dt)$, with the magnetization $\vec{M}$, the gyromagnetic ratio γ, the Gilbert damping parameter α, and the saturation magnetization M_s.[14] The effective field $\vec{H}_{eff}$ contains all coupling contributions and exerts a torque on $\vec{M}$, which initiates its precessional motion, if the Fourier spectrum of the exciting external field pulse comprises significant components of the precessional eigenfrequency of the system.[13] This also holds for a spin torque or a photon angular momentum transfer. Due to the pulsed nature of these excitations, their frequency spectrum usually contains several eigenfrequencies of the system.

In this paper, we quantitatively analyze the magnetization dynamics in micron-sized spin-valve structures. We measured the time-dependent spatial distribution of the magnetization using x-ray magnetic circular dichroism with photoemission electron microscopy (XMCD-PEEM).[26–28] We show that although the averaged magnetization vector reacts on external field pulses according to a single-spin model with critical damping, local modes are excited depending on the shape of the spin-valve structure. The fact that the damping coefficient is independent of the shape favors the model of a nonlocal magnetization damping.

Despite their lateral extension, the magnetization reversal in spin-valve elements was successfully described by a coherent precessional path,[15] assuming a global magnetization value and a high damping coefficient. This finding is surprising, considering the fact that the dynamical behavior of the *local magnetization* driven by the local effective field H_{eff} could influence the response of a spin-valve sensor and the damping coefficient. Besides the shape-induced demagnetization field, H_{eff} contains contributions from the correlated roughness at the FM/NM interfaces[16] and stray fields from inhomogeneously magnetized regions in one of the layers.[17–19] An inhomogeneous interlayer thickness may cause a laterally varying indirect coupling field. Finally, the dynamic magnetization reversal in the free layer may affect the magnetization configuration in the hard layer.[20] The free layer in spin valves was found to show an increased damping coefficient,[18,21] which was attributed to a nonlocal spin pumping model.[22,23] A competing damping process, however, is given by the local excitation of additional short-wavelength and high-frequency spin wave modes.[24,25] In

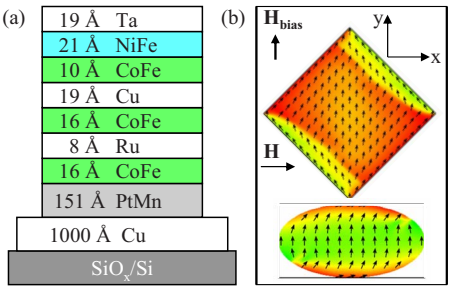

FIG. 1. (Color online) Sketch of the sample geometry as a cross section (a) and top view (b). Snapshots of the micromagnetic simulation (Ref. 30) at 1100 ps shown on the schematic waveguide are discussed in the text. $\mathbf{H}_{\mathrm{bias}}$ and $\mathbf{H}$ denote the exchange bias and pulse field directions, respectively.

general, a local variation of the precessional magnetization motion will lead to unwanted magnetically induced noise in the response of a spin valve[21] or any other fast-switching magnetic structure.[29] Therefore, the understanding of the local magnetization dynamics in complex layer stacks is extremely important, as the dynamics may be determined in a complicated way by the various magnetic coupling effects in a thin film structure.[25] The control of α holds the key for optimized magnetic switching procedures.[21]

The samples studied stand as examples of complex magnetic layer stacks and represent advanced spin-valve structures (Fig. 1), designed to optimize the GMR effect. They have been successfully implemented into commercial devices by NAOMI/Sensitec (Mainz). The layer stack was deposited on Cu(100 nm)/SiO_x/Si(111) substrates. Subsequent lithography steps lead to the final structure of a coplanar waveguide (20 μm width of the central lead) with microscopic spin-valve elements of several shapes on top. The magnetically soft CoFe/NiFe free layer is separated from the CoFe hard layer by an ultrathin Cu interlayer providing an antiferromagnetic coupling field of 0.6 mT, as derived from the easy axis loop ($H \| y$). The hard axis loop ($H \| x$) reveals a nearly reversible magnetization rotation. From the initial slope of the hard axis loop, we deduce a total anisotropy field of 1.5 mT. The difference might be ascribed to a uniaxial anisotropy due to the field applied during the sample preparation.

The time-resolved experiments were performed by stroboscopic illumination of the sample with circular polarized ($\vec{P}_{circ}$) x-ray pulses at the Ni L_3 absorption edge produced by electron bunches in the synchrotron ring (t_{FWHM}=3 ps, low-α mode at BESSY II, Berlin) with a repetition rate of 500 MHz. In this way, the response of the element is tested via the top electrode of the spin-valve structure. The field pulses are synchronized by means of an electronic delay t, which was varied in steps of 20 ps, matching the overall time resolution.[28] For each image, the sample is thus excited and probed every 2 ns. To acquire an image, we typically integrate the signal for 30 s, thus averaging over 1.5×10^{10} pump-probe cycles. The gray level in the XMCD-PEEM images is given by the scalar product $M_x \propto \vec{M}\cdot\vec{P}_{circ}$.

In the ground state, the exchange bias field forces the microscopic SV elements into an almost uniform magnetization state (weak contrast in Fig. 2, 0 ps). Only in the vicinity of the edges does the magnetization turn parallel to the boundaries, thus comprising a positive (negative) value of $M_x(t)$ and avoiding stray field energy. The magnetic field pulse of amplitude of 1 mT rotates the magnetization $\vec{M}(\vec{r},t)$ into the direction of the external field. After the pulse has passed, $\vec{M}(\vec{r},t)$ rotates through the equilibrium position into the opposite direction and finally back to its initial direction. In order to test the homogeneity of the precession across the structure, we analyze line profiles taken along the diagonal of the structures [Fig. 3(a)]. These profiles reveal that $\vec{M}(\vec{r},t)$ is not phase coherent in the case of the square. After an almost homogeneous initial rotation toward the field direction (x), $M_x(t)$ starts to decrease at 600 ps in the central part faster than in the two areas close to the corners (indicated by the vertical lines). This incoherent rotation leads to the wave pattern at 1000 ps comprising two nodes along the x diagonal. Then, with increasing delay time, $M_x(t)$ increases faster in the center, resulting in the two separated minima (occurring at the same position as the maxima observed at 400–1000 ps). Finally, $M_x(t)$ again reaches a homogeneous value across the square at 1800 ps. In contrast, similar profiles across the ellipse shown in Fig. 3(b) reveal an almost coherent rotation of $\vec{M}(\vec{r},t)$ indicated by an almost constant value of $M_x(t)$ for fixed delay times.

Figure 4(b) compares the time dependence of $M_x^m(t)$ averaged over the total field of view with the local value $M_x^s(t)$ [$M_x^e(t)$] measured in the central circular area of the square (ellipse) (indicated in Fig. 2). For better comparison, $M_x^m(t)$ was normalized to the same maximum amplitude as the local values. At first glance, the time dependences $M_x^i(t)$ are close to each other and resemble that of a critically damped oscillation. The simultaneous fluctuations of $M_x^i(t)$ near 600 and

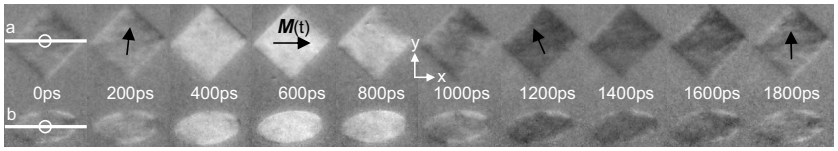

FIG. 2. Sequence of selected snapshots of the XMCD contrast of a quadratic (5×5 μm^2) and elliptical (6×3 μm^2) spin-valve element acquired simultaneously at the indicated time delay. The external field (amplitude $\mu_0 H$=1 mT) with time dependence according to Fig. 4(a) is applied along the horizontal (x) axis. The easy magnetization direction points along the perpendicular (y) axis. The gray level indicates the magnetization component along the x axis. For some delay times, the magnetization vector in the center of the square particle is indicated by arrows.

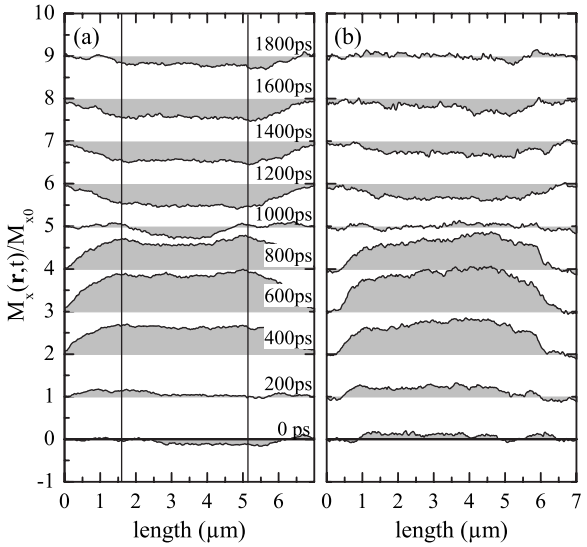

FIG. 3. Profiles along the lines (a) and (b) indicated in Fig. 2 at the designated time delays. The magnetization component $M_x(\vec{r})$ is roughly calibrated by the maximum XMCD value M_{x0} measured during the sequence of images. For clarity, the profiles are shifted by unity.

1500 ps are caused by adjustments of the electron optics and beam injection at the synchrotron.

The local variations of $M_x(t)$ are emphasized in the difference image shown as an inset in Fig. 4(b) and by the differences $\Delta M_x(t)=M_x^i(t)-M_x^m(t)$, revealing the true discrepancies between averaged and local magnetization dynamics [Fig. 4(c)]. Residual small edge domains that do not participate in the magnetization rotation cause the positive (negative) constant offset of $\Delta M_x^i(t)$ for the ellipse (square). For the ellipse, $\Delta M_x^e(t)$ reveals a broad maximum coinciding with the strong counterclockwise rotation of $\vec{M}(\vec{r},t)$. This behavior indicates a slower rebound of $\Delta M_x^e(t)$ that can be explained by the attenuation of the bias field by the in-plane demagnetization field of the ellipse, which reveals a hard axis parallel to the bias field. Contrarily, $\Delta M_x^s(t)$ shows an oscillation with a frequency of 1.7 GHz. The difference image shown in the inset of Fig. 4(b) relates this frequency to a spin wave mode identified by the two circularly shaped black areas coinciding with the maxima (minima) of the profiles indicated by the vertical lines in Fig. 3(a). Because of the presence of this higher-order spin wave mode, the magnetization vector rotates faster in the region of these maxima (minima) compared to the nodes positioned in between, thus leading to a change of the rotation direction of the magnetization vector across the square particle for certain delay times. The wavelength of this mode along the diagonal amounts to 3.5 μm, i.e., half the value of the diagonal of the square particle. For the elliptical particle, such a higher-order mode is not observed. The direction magnetization rotation does not change sign across the diameter.

The fundamental eigenmode frequency of the square estimated from a similar measurement using smaller and shorter field pulses takes a value of $f=0.8$ GHz in the field-free time range. Neglecting lateral demagnetizing fields and assuming

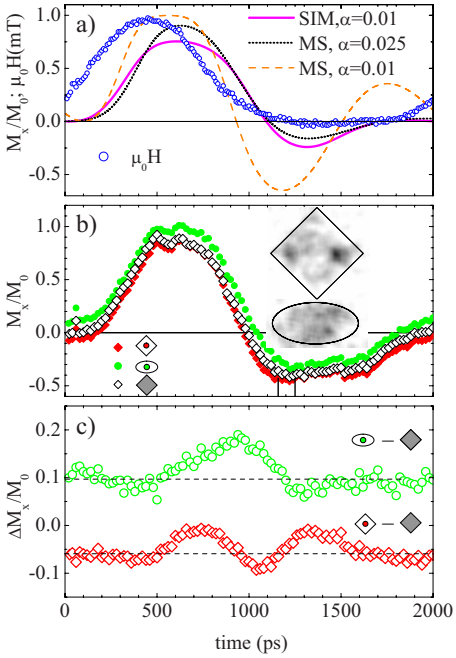

FIG. 4. (Color online) (a) Field pulse $H_x(t)$ (open circles) with a repetition rate of 0.5 GHz. Magnetization component $M_x(t)$ predicted by the macrospin (MS) model with low (dashed line) and high (dotted line) damping coefficients. $M_x(t)$ calculated by a micromagnetic simulation (Ref. 30) (SIM) for the square pattern is shown by the full line. (b) $M_x(t)$ averaged over the complete field of view [$M_x^m(t)$, open diamond] and in the central area of the square spin-valve platelet [$M_x^s(t)$, full diamond] and of the elliptical particle [$M_x^e(t)$, full circle] versus time delay. The inset shows a difference image between images acquired at times 1160 and 1260 ps. (c) Magnetization variation $\Delta M_x=M_x^i-M_x^m$ for the central areas of the square (open diamond) and the ellipse (open circle).

a macrospin model, the ferromagnetic resonance frequency for exchange biased films is given by

$$2\pi f=\gamma\sqrt{M_s H_A}, \tag{1}$$

with the gyromagnetic ratio γ and $H_A=H_{\text{bias}}+H_s$ including the exchange bias field H_{bias} and an induced in-plane uniaxial anisotropy H_s. For the saturation magnetization $\mu_0 M_s=1.3$ T, we assumed a weighted average of the bulk values for FeNi and CoFe. Under these conditions, the observed eigenmode frequency corresponds to $H_A=0.6$ mT, in agreement with the quasistatic value of H_{bias} derived from the easy axis magnetization curve.

Single-spin (macrospin) simulations considering the complete magnetic layer stack suggest that the rotation of the pinned layer can be safely neglected. The single-spin model has to be adjusted with a high damping constant of $\alpha=0.025$ and $H_A=0.6$ mT in order to approximate $M_x(t)$ [see Fig. 4(a)]. The damping coefficient agrees with results reported in Ref. 18 for the free layer of a very similar spin-valve element. Contrarily, a damping constant of $\alpha=0.01$, which is closer to values reported for the unbiased free layers,[19] results in a maximum of $M_x(t)$ at 1800 ps (dashed curve) that is clearly not observed in our experiment. A full

micromagnetic simulation[26] of the square using $\alpha=0.01$ and replacing the exchange bias stack by a constant field yields a closer agreement with the experimental results. It also reproduces the relatively large rebound maximum of $M_x(t)$ in contrast to the macrospin result.

The snapshots of the micromagnet simulation [Fig. 1(b)] reveal the characteristic differences between the square and the ellipse in agreement with the experiment: While the magnetization has already rotated back into the equilibrium position in the center of the square, $\vec{M}$ still shows a clockwise rotated position toward the left and right corners. In contrast to this behavior, the ellipse shows a homogeneous magnetization direction along the long axis. Clearly, the shape is responsible for these differences.

In conclusion, using time-resolved microscopy, we find that the magnetization dynamics of the free layer of a spin-valve stack deviates significantly from a simple phase coherent rotation. The dynamic response of the free layer is a superposition of an averaged critically damped precessional motion and localized spin wave modes, which strongly depend on the shape of the micropattern. A micromagnetic simulation qualitatively reproduces the observed spin wave mode for the square platelet. In principle, higher-order spin wave modes provide an additional efficient channel for energy dissipation and thus should result in a higher effective damping coefficient, as observed in our experiments. We found the damping coefficient to be independent of the shape of the spin-valve element, thus favoring the model of nonlocal magnetization damping.

This work was supported by the DFG (SPP 1133 and SFB 491) and BMBF (03N6500). Thanks are due to the BESSY staff and, in particular, to D. Schmitz (HMI, Berlin) for excellent support.

*elmers@uni-mainz.de

[1] P. Grünberg, R. Schreiber, Y. Pang, M. B. Brodsky, and H. Sowers, Phys. Rev. Lett. **57**, 2442 (1986).
[2] M. N. Baibich, J. M. Broto, A. Fert, F. Nguyen Van Dau, F. Petroff, P. Etienne, G. Creuzet, A. Friederich, and J. Chazelas, Phys. Rev. Lett. **61**, 2472 (1988).
[3] G. Binasch, P. Grünberg, F. Saurenbach, and W. Zinn, Phys. Rev. B **39**, 4828 (1989).
[4] R. Coehoorn, in *Handbook of Magnetic Materials*, edited by K. H. J. Buschow (Elsevier Science, Amsterdam, 2003), Vol. 15.
[5] J. Raabe, C. Quitmann, C. H. Back, F. Nolting, S. Johnson, and C. Buehler, Phys. Rev. Lett. **94**, 217204 (2005).
[6] K. Perzlmaier, M. Buess, C. H. Back, V. E. Demidov, B. Hillebrands, and S. O. Demokritov, Phys. Rev. Lett. **94**, 057202 (2005).
[7] S.-B. Choe, Y. Acremann, A. Scholl, A. Bauer, A. Doran, J. Stohr, and H. A. Padmore, Science **304**, 420 (2004).
[8] H. Stoll *et al.*, Appl. Phys. Lett. **84**, 3328 (2004).
[9] J. P. Park, P. Eames, D. M. Engebretson, J. Berezovsky, and P. A. Crowell, Phys. Rev. B **67**, 020403(R) (2003).
[10] B. C. Choi, M. Belov, W. K. Hiebert, G. E. Ballentine, and M. R. Freeman, Phys. Rev. Lett. **86**, 728 (2001).
[11] E. B. Myers, D. C. Ralph, J. A. Katine, R. N. Louie, and R. A. Buhrman, Science **285**, 867 (1999).
[12] W. Weber, S. Riesen, and H. C. Siegmann, Science **291**, 1015 (2001).
[13] S. O. Demokritov, B. Hillebrands, and A. N. Slavin, Phys. Rep. **348**, 441 (2001).
[14] L. Landau and E. Lifshitz, Phys. Z. Sowjetunion **8**, 153 (1935); T. L. Gilbert, Phys. Rev. **100**, 1243 (1955).
[15] H. W. Schumacher, C. Chappert, P. Crozat, R. C. Sousa, P. P. Freitas, J. Miltat, J. Fassbender, and B. Hillebrands, Phys. Rev. Lett. **90**, 017201 (2003).
[16] Y. Pennec, J. Camarero, J. C. Toussaint, S. Pizzini, M. Bonfim, F. Petroff, W. Kuch, F. Offi, K. Fukumoto, F. Nguyen Van Dau, and J. Vogel, Phys. Rev. B **69**, 180402(R) (2004).
[17] R. Schäfer, R. Urban, D. Ullmann, H. L. Meyerheim, B. Heinrich, L. Schultz, and J. Kirschner, Phys. Rev. B **65**, 144405 (2002).
[18] H. W. Schumacher, C. Chappert, P. Crozat, R. C. Sousa, P. P. Freitas, and M. Bauer, Appl. Phys. Lett. **80**, 3781 (2002).
[19] M. C. Weber, H. Nembach, B. Hillebrands, and J. Fassbender, J. Appl. Phys. **97**, 10A701 (2005).
[20] L. Thomas, M. G. Samant, and S. S. P. Parkin, Phys. Rev. Lett. **84**, 1816 (2000).
[21] S. E. Russek, R. D. McMichael, M. J. Donahue, and S. Kaka, *Spin Dynamics in Confined Magnetic Structures*, Topics in Applied Physics Vol. 87 (Springer, Berlin, 2003), p. 93.
[22] L. Lagae, R. Wirix-Speetjens, W. Eyckmans, S. Borghs, and J. De Boeck, J. Magn. Magn. Mater. **286**, 291 (2005).
[23] Y. Tserkovnyak, A. Brataas, G. E. W. Bauer, and B. I. Halperin, Rev. Mod. Phys. **77**, 1375 (2005).
[24] G. Eilers, M. Lüttic, and M. Münzenberg, Phys. Rev. B **74**, 054411 (2006).
[25] W. K. Hiebert, G. E. Ballentine, L. Lagae, R. W. Hunt, and M. R. Freeman, J. Appl. Phys. **92**, 392 (2002).
[26] A. Krasyuk, A. Oelsner, S. A. Nepijko, A. Kuksov, C. M. Schneider, and G. Schönhense, Appl. Phys. A: Mater. Sci. Process. **A76**, 863 (2003).
[27] A. Krasyuk, F. Wegelin, S. A. Nepijko, H. J. Elmers, G. Schönhense, M. Bolte, and C. M. Schneider, Phys. Rev. Lett. **95**, 207201 (2005).
[28] G. Schönhense, H. J. Elmers, S. A. Nepijko, and C. M. Schneider, Adv. Imaging Electron Phys. **142**, 159 (2006).
[29] B. Hillebrands and J. Fassbender, Nature (London) **418**, 493 (2002).
[30] Parameters used for the simulations were $A=1.3\times10^{-11}$ J/m, $M_s=10.4\times10^5$ kA/m, $\alpha=0.01$, and $H_y=0.6$ mT. The particle size and $H_x(t)$ are similar to those in the experiment: the cell size is 20 nm (http://math.nist.gov/oommf/).